Journal of Power Sources 247 (2014) 70–77

Contents lists available at ScienceDirect

Journal of Power Sources

journal homepage: www.elsevier.com/locate/jpowsour

Pd and PdCo alloy nanoparticles supported on polypropylenimine dendrimer-grafted graphene: A highly efficient anodic catalyst for direct formic acid fuel cells

Hadi Hosseini, Mojtaba Mahyari, Akbar Bagheri*, Ahmad Shaabani

Department of Chemistry, Shahid Beheshti University, G. C., P.O. Box 19396-4716, Tehran, Iran

HIGHLIGHTS

- Pd and PdCo nanoparticles were supported on polypropylenimine dendrimer–grafted graphene (Pd and PdCo/PPI-g-G).
- The PdCo/PPI-g-G shows a good activity for formic acid electrooxidation.
- The kinetic parameters were estimated under the quasi steady-state conditions.

GRAPHICAL ABSTRACT

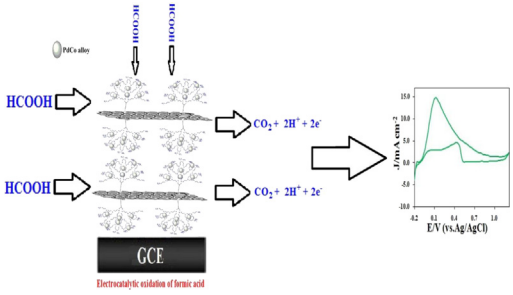

ARTICLE INFO

Article history:
Received 23 March 2013
Received in revised form
23 July 2013
Accepted 17 August 2013
Available online 30 August 2013

Keywords:
Fuel cells
Electrocatalysts
Metal nanoparticles
Palladium and cobalt nanoparticles
Formic acid oxidation

ABSTRACT

For the first time, Pd and PdCo alloy nanoparticles supported on polypropylenimine dendrimer-grafted graphene (Pd and PdCo/PPI-g-G) are prepared and characterized with Fourier transform infrared spectroscopy (FTIR), nuclear magnetic resonance spectroscopy (NMR), thermogravimetric analysis (TGA), X-ray diffraction (XRD), X-ray photoelectron spectroscopy (XPS), and transmission electron microscopy (TEM). The electrocatalytic activity of Pd and PdCo/PPI-g-G are investigated in terms of formic acid electrooxidation in H_2SO_4 aqueous solution. The PdCo/PPI-g-G shows much higher formic acid oxidation activities in comparison with Pd/PPI-g-G, and it is more resistant to the surface poisoning. This improved electrocatalytic performance may be due to the fine dispersion of PdCo alloy nanoparticles and bifunctional effect. The kinetic parameters such as charge transfer coefficient and the diffusion coefficient of formic acid are estimated under the quasi steady-state conditions.

© 2013 Elsevier B.V. All rights reserved.

1. Introduction

Fuel cells are modular electrochemical devices which directly convert chemical energy into electrical energy with high conversion efficiency and low environmental pollution. Over the past few decades, Direct formic acid fuel cells (DFAFCs) are attractive as one of the promising energy sources for stationary and portable electronic device applications [1–8]. Formic acid is non-toxic, food additive, inflammable, and does not require special device for storage and transportation [9]. Moreover, DFAFCs have the potential to achieve better performance than direct methanol fuel cells (DMFCs). Formic acid has two orders of magnitude smaller crossover flux through a Nafion® membrane than methanol allowing the use of highly concentrated fuel solutions in DFAFCs [9]. The DFAFCs can have higher power density than direct DMFCs. In addition, the electro-oxidation of formic acid occurs at a less positive potential

* Corresponding author. Tel.: +98 21 29903251; fax: +98 21 22431661.
E-mail address: akbr_bagheri@yahoo.com (A. Bagheri).

0378-7753/$ – see front matter © 2013 Elsevier B.V. All rights reserved.
http://dx.doi.org/10.1016/j.jpowsour.2013.08.061

than methanol [10]. Therefore, DFAFCs have many advantages over DMFCs. There are two types of reaction mechanism for formic acid electro-oxidation, namely "direct pathway mechanism" and "dual pathway mechanism (or CO pathway mechanism)" [9]. It is desirable to develop an electrocatalyst system that the electro-oxidation of formic acid goes through "direct pathway mechanism"; because this reaction pathway involves no significant CO poisoning. Recent progress in formic acid electro-oxidation has revealed that the Pd or Pd-based electrocatalysts possess better performances towards the anodic oxidation of formic acid in DFAFCs compared with Pt or Pt-based electrocatalysts [9,11,12]. In addition, recent efforts in formic acid oxidation have been focused on combination of a second component (such as Pt, Au, Co, Ir, Cu, etc.) with Pd which is effective strategy to further enhance its catalytic activity and durability [13–19]. The main reason for enhancement in catalytic activity of Pd in the presence of second element is due to the weakening of the adsorption of reaction intermediates on catalyst surface, which has been illustrated by the electronic, strain, or alloying effects [19,20].

Few papers have recently reported different PdCo bimetallic alloys that enhance the Pd electrocatalytic activity and stability for formic acid oxidation [17,21–25]. The sizes of Pd nanoparticles significantly affect the electrooxidation of formic acid [26]. Thus, the control of the sizes of Pd nanoparticles has attracted particular interest due to their increased surface area and the number of edge and corner atoms, which significantly improve their catalytic properties [26]. To control the size and to avoid the aggregation of the Pd nanoparticles, catalysts stabilizers such as multi-walled carbon nanotubes [6], helical carbon nanofibers [27], high active carbon [16], graphene oxide [28], and SnO_2 nanospheres [29] which make a high dispersion of small Pd nanoparticles were used. Although these catalysts stabilizers provide relatively good catalytically efficient nanoparticles, using dendrimers, a unique class of polymers, has more benefits such as obtaining high dispersion, high loading level, high stability, and controlled particle sizes and morphologies of catalyst nanoparticles [30–33]. Polypropylenimine (PPI) dendrimer is an attractive dendrimer which acts as good stabilizer and linker for the incorporation of metal nanoparticles on the surface of support materials for different catalysis applications [33]. Recently, graphene has become one of the most exciting topics of research with potential applications in various fields such as solar cells, electronic devices, energy storage and conversion devices, biosciences, and biotechnologies [8,34–36]. Graphene also is attractive solid support for catalysts due to its unique properties and surface structure. The attachment of dendrimers to the surface of graphene is a good strategy used to fabricate new catalysts stabilizers with unique properties for the formic acid electro-oxidation. In this work, we prepared Pd and PdCo alloy nanoparticles supported on polypropylenimine dendrimer–grafted graphene (Pd and PdCo/PPI-g-G). The activity of new electrocatalytic toward formic acid electro-oxidation was tested by cyclic voltammetry (CV), linear sweep voltammetry (LSV) and chronoamperometry techniques. The new electrocatalysts exhibited excellent performances for formic acid electro-oxidation.

2. Experimental

2.1. Apparatus and materials

AA-680 Shimadzu (Kyoto, Japan) flame atomic absorption spectrometer (AAS) with a deuterium background corrector was used for determination of Pd (0) and Co (0). IR spectra were recorded on a Bomem MB-Series FT-IR spectrophotometer. A transmission electron microscopy (TEM) analysis was performed by ZEISS EM-900 at an acceleration voltage of 80 kV. ^{1}H NMR spectra were recorded with a BRUKER DRX-300 AVANCE spectrometer and DMSO-d_6 was used as a solvent. X-ray photoelectron spectroscopy (XPS) analysis was performed using a VG multilab 2000 spectrometer (ThermoVG scientific) in an ultra high vacuum. Ultrasonic bath (EUROSONIC® 4D ultrasound cleaner with a frequency of 25 kHz) was used to disperse materials in solvent. Thermogravimetric analysis (TGA) was carried out using STA 1500 instrument at a heating rate of 10 °C min^{-1} in air. X-ray powder diffraction (XRD) data were collected on an XD-3A diffractometer using Cu Kα radiation. All reagents used were of analytical grade, and all solutions were prepared with double distilled water.

2.2. Electrochemical measurements

Electrochemical experiments were performed using a μAutolab Type III electrochemical system. A conventional three-electrode cell consisting of a glassy carbon working electrode modified with electrocatalyst sample, a platinum wire counter electrode, and a saturated Ag/AgCl reference electrode were used for voltammetric experiments. The current was normalized to the apparent surface area of the glassy carbon electrode (0.0314 cm^2). A glassy carbon electrode (GCE) was cleaned by polishing with 0.05 μm alumina slurry on a polishing cloth to create a mirror finish; the electrode was then sonicated with absolute ethanol and double-distilled water for about 5.0 min, respectively. It was rinsed thoroughly with double-distilled water and then dried under ambient temperature. The ink of electrocatalyst samples containing 2.0 mg ml^{-1} in DMF using 30 min ultrasonic agitation was prepared. After the electrode surface was air dried, 5.0 μL of ink was cast onto the surface of the pretreated GC electrode with a microsyringe and then it was dried in air. All experiments were done at room temperature (25.0 ± 1 °C). The electrochemical measurements were performed in 0.5 M H_2SO_4 + 0.1 M formic acid solution.

2.3. Preparation of catalysts

2.3.1. Preparation of 1,3-diamine-functionalized graphene

At the first step, the graphene oxide (GO), prepared by Hummer method [37], was functionalized by malononitrile [38]. Then, the product was reduced as the following procedure; $CoCl_2 \cdot 6H_2O$ (23.8 g, 100.0 mmol) in MeOH (300.0 mL) and $NaBH_4$ (19.0 g, 500.0 mmol) were added to the malononitrile-functionalized graphene and the reaction mixture was stirred at 20 °C for 24 h. Then, the reaction mixture was acidified with 3 N HCl (100.0 mL). Finally, the mixture was stirred at ambient temperature for 4 days to ensure reaction completion. The product was filtered under vacuum, washed with methanol and acetone and dried under vacuum for 24 h.

2.3.2. Preparation of PPI-g-G hybrid materials

Various generation (First-, second- and third-generation) of the PPI dendrimers were synthesized on the amino functionalized graphene. The amino functionalized graphene oxide (0.8 g) was added in portions at ambient temperature with stirring to acrylonitrile (3.4 mL, 80.0 mmol) and methanol (10.0 mL) in a 100 mL round-bottomed flask. The reaction mixture was stirred at room temperature under nitrogen atmosphere for 5 days. After completion the reaction, excess reactants and solvent were removed under vacuum. The obtained product was washed with methanol and acetone and was dried under vacuum for 24 h. Then, $CoCl_2 \cdot 6H_2O$ (23.8 g, 100.0 mmol) in MeOH (300.0 mL) and $NaBH_4$ (19.0 g, 500.0 mmol) were added to the product of previous step; the mixture was stirred at 20 °C for 24 h. After that, the resulting mixture was acidified with 3 N HCl (100.0 mL). Finally, the reaction mixture was stirred at room temperature for 4 days to ensure

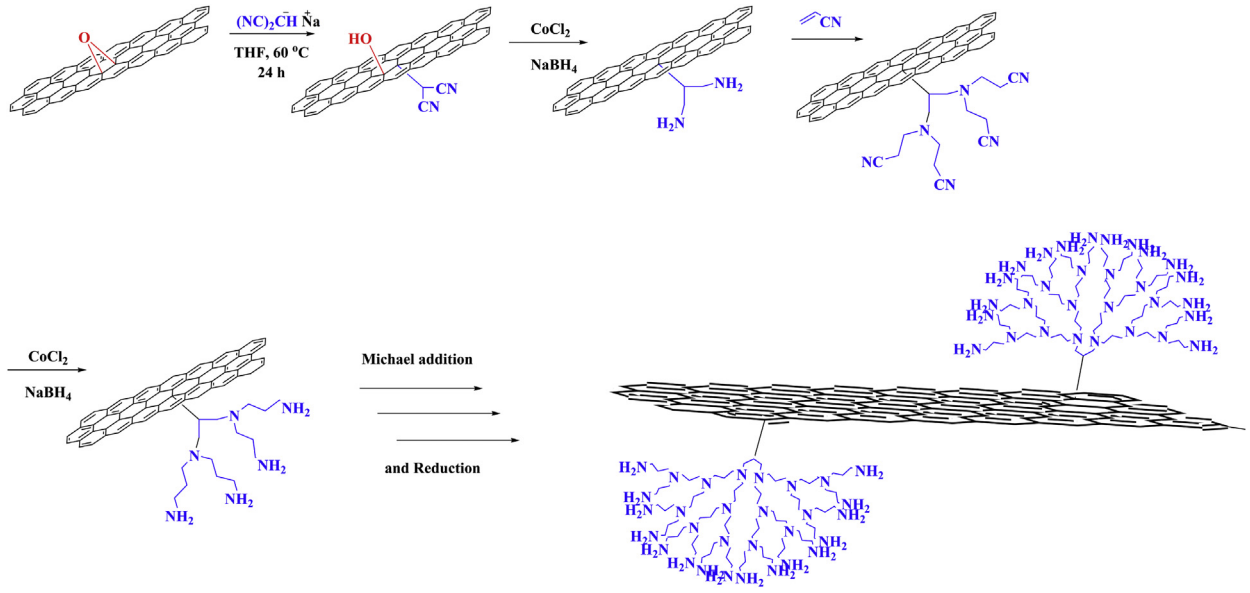

Scheme 1. Synthesis route of polypropyleneamine dendrimer growth on graphene.

reaction completion (Scheme 1). Next, the product was filtered under vacuum, washed with ethanol and water and dried under vacuum at 50 °C for 4 h [39,40]. Then the synthesis, titration method [41] was used to calculate the amount of free primary amines in the periphery of the dendrimer (Table S-1).

2.3.3. *Preparation of PdCo/PPI-g-G hybrid materials*

First, aqueous solution of $PdCl_2$ (0.1 g in 3.0 mL) and PPI-g-graphene (0.2 g in 10.0 mL) were mixed and placed in an ultrasonic bath (50 KHz) for 20 min to well disperse metal ions in the dendritic shell of hybrid material. Then, the mixture was stirred for 30 min, aqueous solution of $CoCl_2$ (0.2 g in 3.0 mL) was added. The solution was placed in an ultrasonic bath for 20 min, followed by $NaBH_4$ (1.0 M, 10.5 mL) solution in 0.3 M aqueous NaOH was added the reaction mixture. After stirring for several hours, it was filtered under vacuum, washed well with ethanol and water and dried under vacuum at 50 °C for 4 h.

2.4. *Formic acid decomposition*

The catalytic decomposition of formic acid was carried out in a double-walled thermostatically controlled reaction vessel by stirring the mixture of the aqueous suspension of 2 mL of 1 M formic acid and 10 mg of PdCo/PPI-g-G at a given temperature (40 °C) with a reflux condenser, which is connected to an automatic gas burette, where the gases are collected. The generated gases were analyzed by gas chromatography (Shimadzu 8A) equipped with a TCD detector.

3. Results and discussion

The steps of dendrimer grown on graphene and subsequent loading of Pd and Co have been shown in Schemes 1 and 2. For the preparation of functionalized graphene by amine through covalent bonding, at the first, malononitrile as carbon nucleophile in basic conditions was attacked to epoxy sits on the surface graphene oxide and then nitrile groups are reduced. Consequently, the PPI dendrimer up to third generation were grown on the surface of graphene to obtain the PPI-g-G hybrid materials employing a divergent route starting from the nitrile-functionalized graphene. The FT-IR spectroscopy was used as a first technique to confirm the formation the three generation of the dendrimer (Fig. S-1). Increasing the peaks intensity have confirmed for growing generation dendrimer. The broad band at 3430 cm^{-1} is due to the $-NH_2$ stretching, the absorptions at 2800 and 3000 cm^{-1} are attributed to the C—H bending of the CH_2 groups' dendrimer. In addition, the band at 2192 cm^{-1} is assigned to the CN group that confirmed malononitrile-functionalized graphene (Fig. S-1B). The increase in the relative intensity of the above mentioned absorptions indicates that each generation of dendrimer was successfully constructed on the surface of graphene. ^1H NMR results provide valuable information on the functional groups in the third generation PPI-g-G samples in DMSO-d_6. The hydrogen signals of the grafted dendritic units are obviously observable in the corresponding ^1H NMR spectrum. The most shielded signal at 1.1 ppm is attributed to $CH_2CH_2CH_2$ and the next signal at 2.9 ppm could be assigned to CH_2N. The peak at 5.2 ppm was assigned to NH_2 groups (Fig. S-2). The integrations of ^1H NMR of $-NH_2$, $CH_2CH_2C\mathbf{H_2}N$ and $CH_2C\mathbf{H_2}CH_2N$ are in the ratio of 1:3.35:1.61, respectively. These values confirm the synthesis of third generation of dendrimer, but some deviations are due to defects in the dendrimer structure that are a common issue in the synthesis of dendrimers [42]. Thermogravimetric analysis (TGA) was the next analysis to confirm the quantification of the growth the dendrimer on the surface of the graphene (Fig. S-3). The first decomposition starts between the ranges 100—200 °C with a corresponding weight loss of water. The weight losses observed at 450—600 °C on TGA plots show the average weight loss of 12%, 24%, and 35% for first (C), two (D), and three (E) generations of PPI dendrimer on graphene, respectively. XPS spectrum of PdCo/PPI-g-G hybrid materials was shown in Figs. S-4 and S-5. Since the sensitivity factor of Pd-3d is 2—3 times higher than that of Co-2p [43], the peak area of Pd is larger than Co. The surface Pd and Co are found to be metallic, not oxide, by comparing experimental binding energies (Pd-$3d_{5/2}$: 334.6 eV, Co-$2p_{3/2}$: 777.5 eV) to those of a literature (Pd-$3d_{5/2}$: 334.4 eV, Co-$2p_{3/2}$: 781.5 eV). As for the binding energy of Co, the shift of $2p_{3/2}$ peak to lower energy indicates alloying of Co with Pd [44]. As shown in Fig. 1 the XRD pattern of third generation of PdCo/PPI-g-G hybrid material confirmed the crystalline structure of PdCo bimetallic nanoparticles [45,46]. Scanning electron microscopy (SEM) and

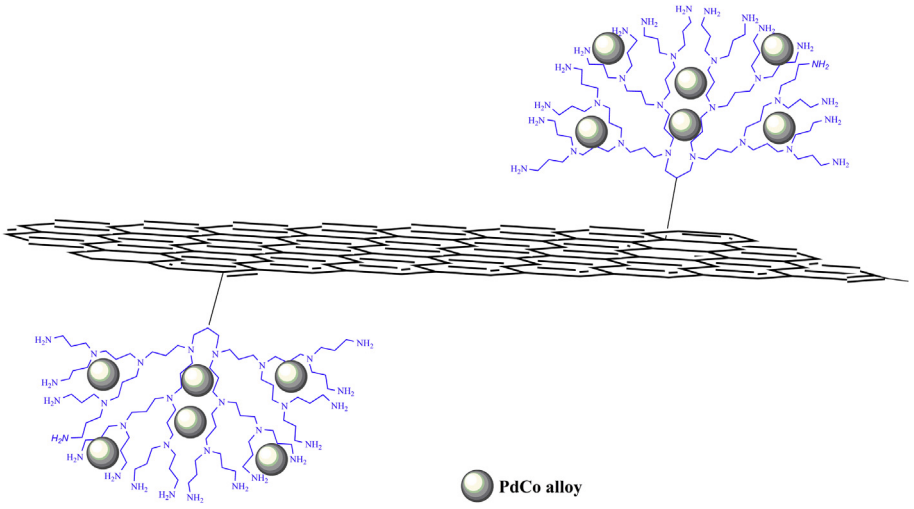

Scheme 2. Synthesis route of PdCo/PPI-g-G hybrid materials.

atomic force microscopy (AFM) (Fig. S-6) of graphene oxide indicated that the thickness of the layer was ~1.0 nm. Furthermore, in Raman spectra of GO (Fig. S-7), two prominent peaks of appearing at around 1354 and 1592 cm^{-1} are related to the D and G modes, respectively. TEM images of graphene oxide (Fig. 2a) and third generation PPI-g-G contained PdCo bimetallic nanoparticles that also showed the uniformly dispersed and the size distribution of supported PdCo alloy nanoparticles in the dendritic on graphene (Fig. 2b). The distribution of the PdCo particles in the PdCo/PPI-g-G hybrid material was obtained by measuring 397 particles randomly and the corresponding histogram of the size distribution is shown in Fig. 2c, indicating that the average particle size of PdCo bimetallic nanoparticles was approximately 2.46 nm. In addition, the energy dispersive X-ray spectroscopy (EDX) of the PdCo/PPI-g-G hybrid materials confirmed the presence of respective elements (Fig. 2d). Finally, cobalt palladium bimetallic dendrimer-encapsulated catalyst has been prepared by the co-complexation method [47]. The amount of Pd and Co in each generation was specified by AAS (Table S-1). As the generation of PPI rises, the loading of Pd and Co nanoparticles was increased. This can be attributed to an exponential increase of amino groups with the increase in the generation of dendrimer.

Electrocatalytic oxidation of formic acid was used to characterize the catalytic activity of the prepared catalysts. Fig. 3 shows the CV profiles of Pd and PdCo/PPI-g-G hybrid materials (third generation) in 0.5 M H_2SO_4 measured in the potential range between −0.2 and 1.2 V. The typical voltammetric curve of Pd in acid media shows the characteristic features of Pd, including the well-defined hydrogen adsorption/desorption peaks in the region of −0.2 V to 0.1 V, double-layer capacitance region (0.2–0.5 V), the oxidation of Pd surface region at the positive potentials (0.53–1.2 V), and subsequent reduction of Pd oxide (0.44 V) in the negative potential scan. As compared to Pd/PPI-g-G, the PdCo/PPI-g-G shows the CV profile with the hydrogen adsorption/desorption current density lower than that recorded for Pd/PPI-g-G, suggesting an inhibition of the hydrogen/desorption on Pd or oxygenated species formation at Co-sites [13]. The CV profiles of Pd/PPI-g-G and PdCo/PPI-g-G catalysts in the solution containing 0.5 M H_2SO_4 and 0.1 M formic acid are shown in Fig. 4. For further comparison, the catalytic activity of PdCo/graphene (PdCo/G) toward formic acid electro-oxidation was also studied (Fig. 4). It was evident that a peak associated with the formic acid oxidation process was observed in both forward and reverse scans. This behavior is typically observed for Pd catalysts [29]. The electro-oxidation peak of formic acid was observed in the forward scan at 0.11, 0.17 and 0.20 V for PdCo/PPI-g-G, Pd/PPI-g-G and PdCo/G, respectively. The peak current density of PdCo/PPI-g-G catalyst was 2.8 times as large as that of the Pd/PPI-g-G catalyst and 4.6 times as large as that of PdCo/G catalyst. According to the oxidation current and potential, the electro-oxidation activity of the catalysts for formic acid was ordered as PdCo/PPI-g-G > Pd/PPI-g-G > PdCo/G catalysts. The difference could be attributed to the alloying effects and a better dispersion of metallic nanoparticles with a lower particle size achieved with the PPI–G supported materials.

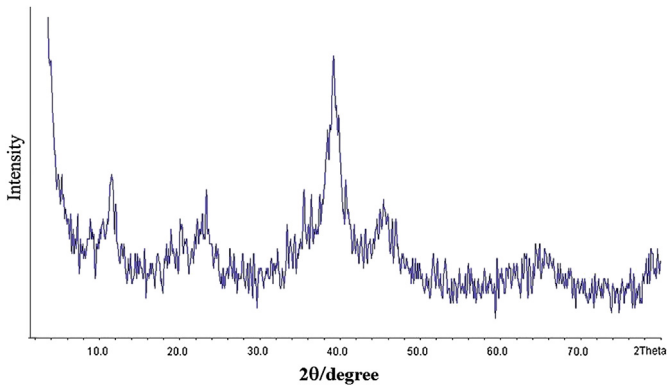

Fig. 1. XRD pattern of PdCo/PPI-g-G hybrid materials.

Furthermore, due to the interaction between Pd and Co in the PdCo/PPI-g-G catalyst, the oxidation reaction of formic acid was facilitated; this behavior is probably due to a direct oxidation pathway to CO_2. Previous studies have also showed that the addition of Co avoids the adsorption of reactive intermediates during the oxidation of formic acid, preventing the accumulation of poisoning-intermediates. Hence, more Pd active sites are available for the direct decomposition of formic acid through the direct pathway [13].

In addition, the effect of various generation (First-, second- and third-generation) of the PdCo/PPI-g-G hybrid materials on the electro-activity of formic acid was also tested by linear sweep voltammetry in the solution containing 0.5 M H_2SO_4 and 0.1 M formic acid (Fig. 5A).

The result clearly demonstrates that the third generation of the PdCo/PPI-g-G hybrid materials has a strong electrocatalytic

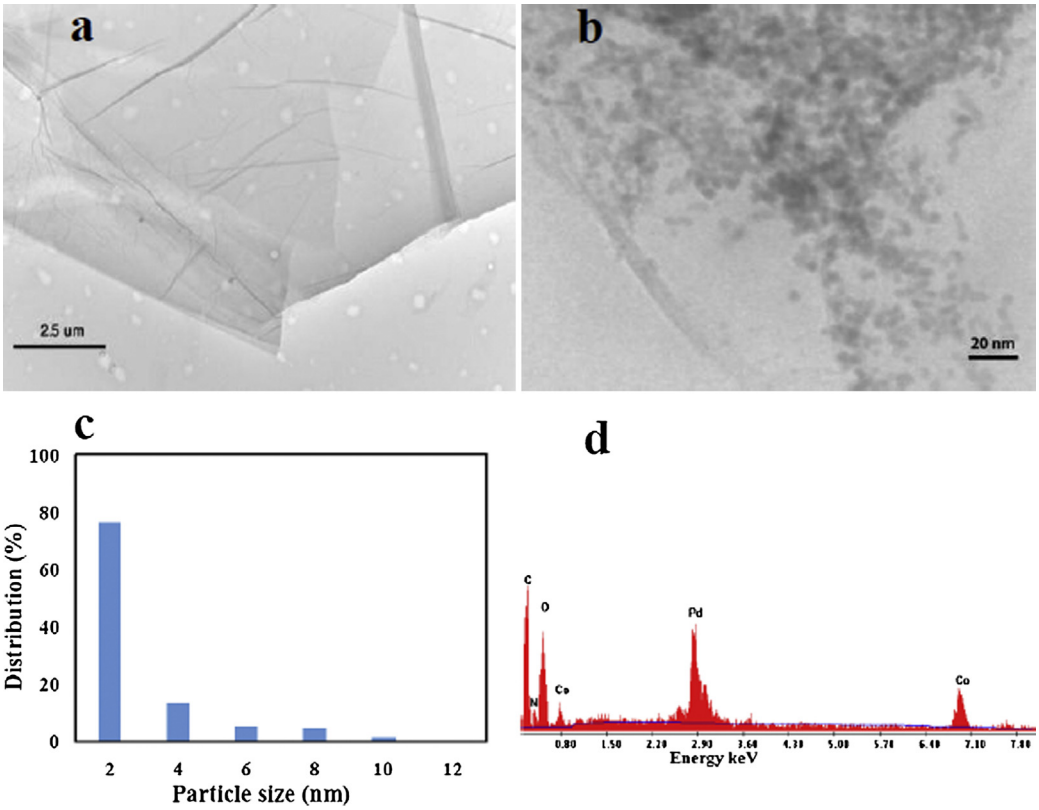

Fig. 2. TEM images of GO (a) and PdCo/PPI-g-G hybrid materials (b). The particle size distribution histogram of PdCo alloy nanoparticles (c) and EDX spectra of PdCo/PPI-g-G hybrid materials (d).

characteristic towards the oxidation of formic acid. As the generation of PPI rises, an exponential increase of amino groups with the increase in the generation of dendrimer was obtained and the loading of Pd and Co nanoparticles was increased and more formic acid amounts were oxidized.

Moreover, the catalytic efficiency of PdCo/PPI-g-G was compared to some reported catalysts [10,18,19,25–29,48–52] in terms of peak current density (Table 1). Table 1 demonstrates that the PdCo/PPI-g-G shows better catalytic efficiency and ability as compared to the other listed catalysts.

The oxidation of formic acid at the PdCo/PPI-g-G catalyst electrode is a completely irreversible kinetic process. For further study, the effect of potential scan rates on the electrochemical behavior of formic acid oxidation at the PdCo/PPI-g-G electrode was studied by CV (Fig. 5B). For an irreversible reaction, the relationship between the peak current density (j_p) and scan rate (υ) can be expressed as:

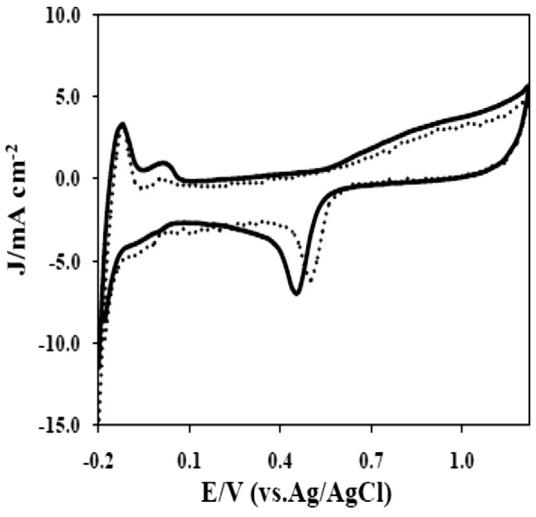

Fig. 3. CV profiles of the Pd/PPI-g-G (···) and PdCo/PPI-g-G (—) catalysts in 0.5 M H_2SO_4 with a scan rate of 10 mV s^{-1}.

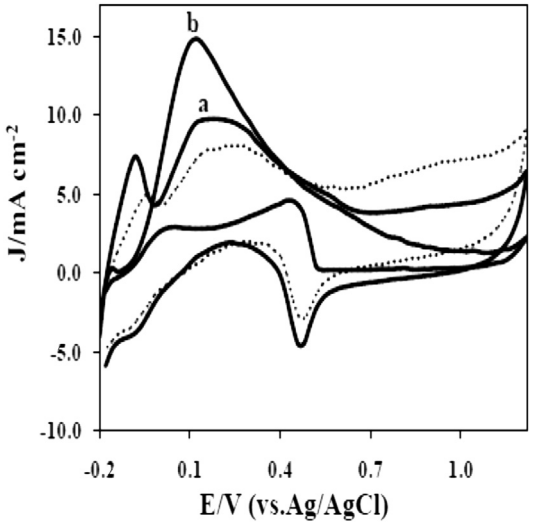

Fig. 4. CV profiles of the PdCo/G (···), Pd/PPI-g-G (a), and PdCo/PPI-g-G (b) catalysts in 0.5 M H_2SO_4 and 0.1 M formic acid with a scan rate of 10 mV s^{-1}.

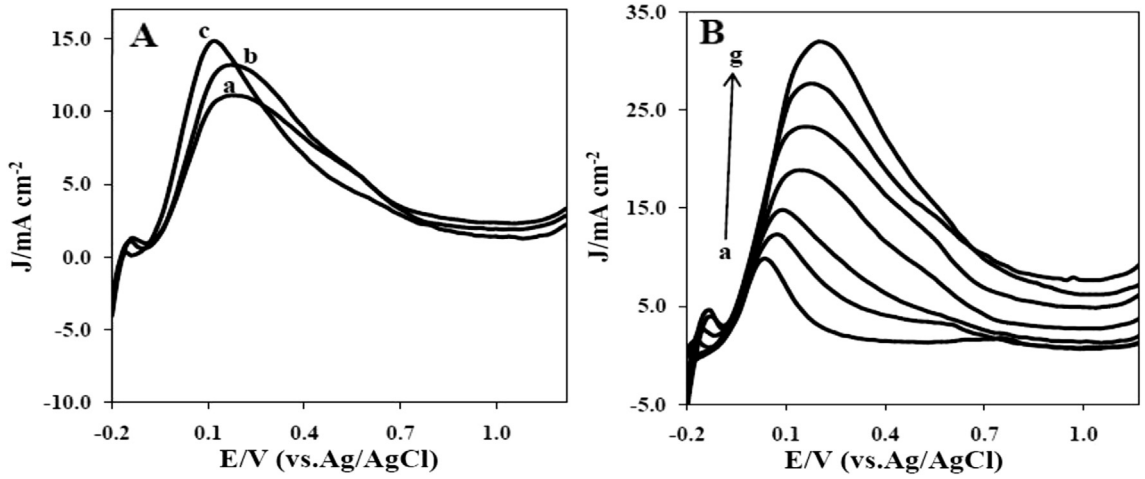

Fig. 5. (A): LSV profiles of the (a) first, (b) second, and (c) third generation of the PdCo/PPI-g-G catalysts in 0.5 M H_2SO_4 and 0.1 M formic acid with a scan rate of 10 mV s^{-1}. (B): LSV profiles of PdCo/PPI-g-G catalysts in 0.5 M H_2SO_4 and 0.1 M formic acid at a different scan rates (from a to g): 2.0, 6.0, 10.0, 20.0, 30.0, 40.0, 50.0 mV s^{-1}.

Table 1
Comparison of catalytic ability of PdCo/PPI-g-G toward the formic acid oxidation with some reported catalysts.

Catalyst	Peak current density (mA cm^{-2})	Scan rate (mV s^{-1})	Supporting electrolyte	Formic acid concentration (M)	Reference
Pd/C catalyst	21.50	50	H_2SO_4 (0.5 M)	0.5	[10]
AuPd Alloy Nanocrystals	≈3.5	50	H_2SO_4 (0.5 M)	0.25	[18]
Nanoporous PdCu alloy	≈6.0	50	$HClO_4$ (0.1 M)	0.1	[19]
Tungsten carbide PdCo nanocatalysts (PdCo/WC-C)	1.7	50	H_2SO_4 (0.5 M)	0.5	[25]
Pd nanoparticles monodispersed on graphene oxide	5.2	50	H_2SO_4 (0.5 M)	0.25	[28]
SnO_2 nanospheres supported Pd catalyst	22.3	50	H_2SO_4 (0.5 M)	0.5	[29]
Carbon-supported Pd–P catalyst	7.57	50	H_2SO_4 (0.5 M)	0.5	[48]
Pt decorated PdAu/C nanocatalysts	12.2	50	$HClO_4$ (0.1 M)	0.5	[49]
Carbon nanotube-supported palladium catalysts	0.18	5	H_2SO_4 (0.5 M)	0.1	[50]
CuPd nanoparticles	≈8.0	100	$HClO_4$ (0.1 M)	0.5	[51]
Pt/Pd nanoparticles	≈2.0	50	H_2SO_4 (0.5 M)	0.25	[52]
PdCo/PPI-g-G	25.5	50	H_2SO_4 (0.5 M)	0.1	This work
	13.1	10			

Approximately (≈).

$$j_p = 2.99 \times 10^5 \, n(\alpha n')^{1/2} C_0 D_0^{1/2} \upsilon^{1/2} \quad (1)$$

where j_p (A cm^{-2}) refers to the peak current density, n is the number of electron transfer, n' is the electron number transferred in the rate-determining step, α is the charge transfer coefficient. D_0 (cm^2 s^{-1}) is diffusion coefficient, C_0 (mol cm^{-3}) is the concentration of formic acid (0.1 M), and υ (V s^{-1}) is the scan rate. Fig. 6A shows the curve of peak current density *vs.* the square root of the scan rate. As it can be seen, the peak current density associated to the formic acid electro-oxidation increases linearly with the square root of scan rate (with the slope of 0.031), which indicates that the electrocatalytic process under study is controlled by diffusion [53]. Furthermore, by increasing the scan rate, the peak potential shifts

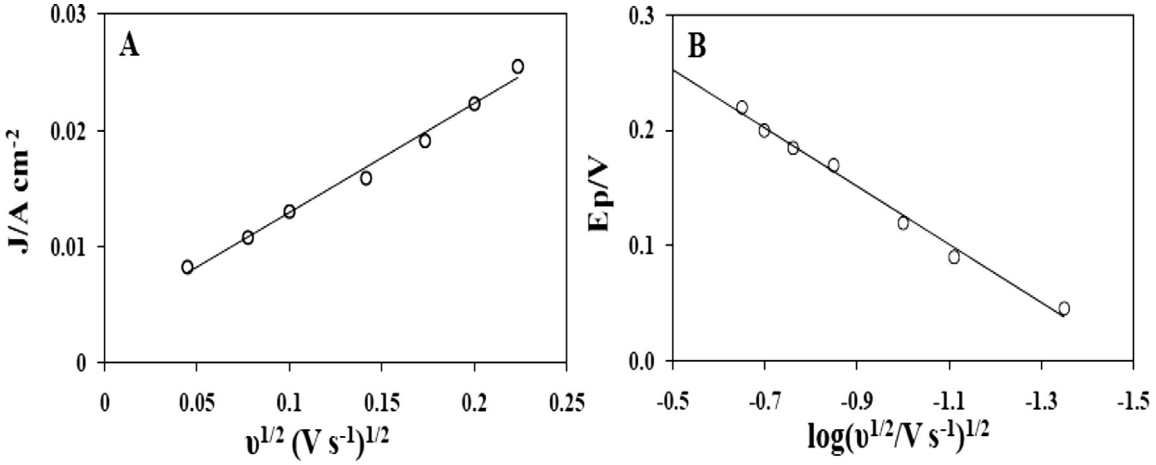

Fig. 6. (A): plot of the peak current density with square root of scan rate. (B): plot of the variation of peak potential with logarithm of the square root of scan rate.

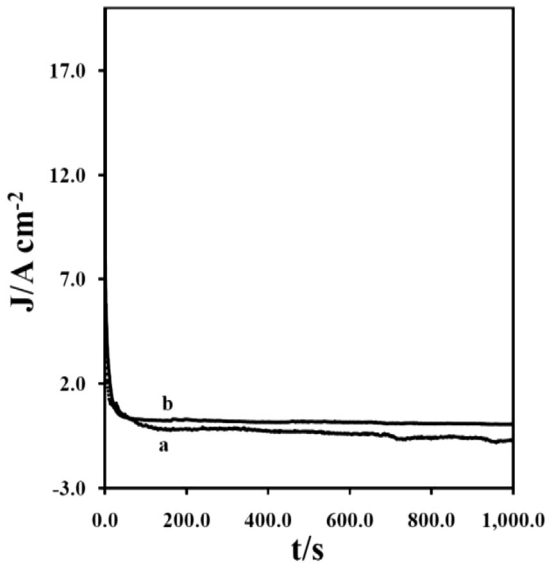

Fig. 7. Chronoamperograms of the Pd/PPI-g-G (a) and PdCo/PPI-g-G (b) catalysts in 0.5 M H_2SO_4 + 0.1 M formic acid.

to more positive values, which this behavior was expect for an irreversible electrode process (Fig. 6B). For a diffusion-controlled and irreversible electrode process, according to Brett and Brett [54], the relationship between the peak potential (E_p) and scan rate (υ) is defined by the following [55]:

$$\left|dE_p/d\log \upsilon^{1/2}\right| = 0.0592/\alpha n' \quad (2)$$

The value of $\alpha n'$ can be easily estimated from the slope of E_p *vs.* $\log \upsilon^{1/2}$. In our system, the slope is 0.251. Generally, n' is assumed [53] to be 1.0 in the rate-determining step. Thus, α was calculated to be 0.235. Based on the slope of the linear relationship between j_p and $\upsilon^{1/2}$ (Fig. 6A and Eq (1)), the value of diffusion coefficient (D_0) of formic acid which is a measurement of the mass-transport rate within the liquid film near the electrode surface can be calculated by LSV. Furthermore, the studies showed that two electron ($n = 2$) were transferred on the mechanism of formic acid oxidation in both direct and indirect pathway [26]. Hence, the value of D_0 was found to be 1.14×10^{-6} cm^2 s^{-1} for PdCo/PPI-g-G catalyst.

To study the electrocatalytic activity and stability of the Pd and PdCo/PPI-g-G electrodes, chronoamperometry was applied and the corresponding current density–time curves are present in Fig. 7. It could be observed from Fig. 7 that the current densities on the PdCo/PPI-g-G, and Pd/PPI-g-G electrodes at 1000 s were 0.98 and 0.23 A cm^{-2}, respectively. Therefore, the PdCo/PPI-g-G catalyst exhibited much higher oxidation current densities than Pd/PPI-g-G at 0.2 V during the period of 1000 s, demonstrating the superior performance of the alloy catalyst. As can be seen (Fig. 7), The degradation in the oxidation current densities and catalytic activity was observed for Pd/PPI-g-G during the period of 1000 s which it was ascribed to the accumulation of poisoning CO-like species, whereas stabilization in the current density observed for PdCo/PPI-g-G was ascribed to the removal of poisoning CO-like species.

Furthermore, in the produced gas mixture released from the decomposition of formic acid on PdCo/PPI-g-G only mixture of H_2 and CO_2 but no CO has been detected by gas chromatography analyses. Typically a ratio of H_2 and CO_2 of 1:1 (±3%) is detected. This indicates that the PdCo/PPI-g-G has a good catalytic selectivity for formic acid dehydrogenation, which is very important for fuel cell applications [56–58].

4. Conclusions

Good dispersion of PdCo alloy nanoparticles over layered polyamidoamine dendrimer-grafted graphene support were prepared and physicochemically characterized by XRD, XPS, FTIR, NMR, and TEM techniques. The PdCo/PPI-g-G exhibit a strong enhanced activity for the anodic formic acid compared with that of Pd/PPI-g-G and PdCo/G catalysts making it a promising anodic catalyst for direct formic acid fuel cells.

Appendix A. Supplementary data

Supplementary data related to this article can be found at http://dx.doi.org/10.1016/j.jpowsour.2013.08.061.

References

[1] C. Rice, S. Ha, R. Masel, P. Waszczuk, A. Wieckowski, T. Barnard, J. Power Sources 111 (2002) 83–89.
[2] C. Rice, S. Ha, R. Masel, A. Wieckowski, J. Power Sources 115 (2003) 229–235.
[3] B. Lim, M. Jiang, P.H. Camargo, E.C. Cho, J. Tao, X. Lu, Y. Zhu, Y. Xia, Science 324 (2009) 1302–1305.
[4] Y. Zhu, S.Y. Ha, R.I. Masel, J. Power Sources 130 (2004) 8–14.
[5] S. Kang, J. Lee, J.K. Lee, S.-Y. Chung, Y. Tak, J. Phys. Chem. B 110 (2006) 7270–7274.
[6] Z. Bai, Y. Guo, L. Yang, L. Li, W. Li, P. Xu, C. Hu, K. Wang, J. Power Sources 196 (2011) 6232–6237.
[7] S. Zhang, S. Guo, H. Zhu, D. Su, S. Sun, J. Am. Chem. Soc. 134 (2012) 5060–5063.
[8] C. Venkateswara Rao, C.R. Cabrera, Y. Ishikawa, J. Phys. Chem. C 115 (2011) 21963–21970.
[9] L. Lu, H. Li, Y. Hong, Y. Luo, Y. Tang, T. Lu, J. Power Sources 210 (2012) 154–157.
[10] N. Cheng, H. Lv, W. Wang, S. Mu, M. Pan, F. Marken, J. Power Sources 195 (2010) 7246–7249.
[11] Y.N. Wu, S.J. Liao, Y.L. Su, J.H. Zeng, D. Dang, J. Power Sources 195 (2010) 6459–6462.
[12] J.L. Haan, R.I. Masel, Electrochim. Acta 54 (2009) 4073–4078.
[13] D. Morales-Acosta, J. Ledesma-Garcia, L.A. Godinez, H. Rodriguez, L. Alvarez-Contreras, L. Arriaga, J. Power Sources 195 (2010) 461–465.
[14] X. Li, I.M. Hsing, Electrochim. Acta 51 (2006) 3477–3483.
[15] X. Wang, Y. Tang, Y. Gao, T. Lu, J. Power Sources 175 (2008) 784–788.
[16] Y. Liu, L. Wang, G. Wang, C. Deng, B. Wu, Y. Gao, J. Phys. Chem. C 114 (2010) 21417–21422.
[17] Z.S. Yang, J.J. Wu, Fuel Cells 12 (2012) 420–425.
[18] L. Zhang, J. Zhang, Q. Kuang, S. Xie, Z. Jiang, Z. Xie, L. Zheng, J. Am. Chem. Soc. 133 (2011) 17114–17117.
[19] C. Xu, Y. Liu, J. Wang, H. Geng, H. Qiu, J. Power Sources 199 (2012) 124–131.
[20] J.R. Kitchin, J.K. Nørskov, M.A. Barteau, J.G. Chen, J. Chem. Phys. 120 (2004) 10240–10246.
[21] X. Wang, Y. Xia, Electrochem. Commun. 10 (2008) 1644–1646.
[22] R. Wang, S. Liao, S. Ji, J. Power Sources 180 (2008) 205–208.
[23] D. Morales-Acosta, M.D. Morales-Acosta, L.A. Godinez, L. Álvarez-Contreras, S.M. Duron-Torres, J. Ledesma-García, L.G. Arriaga, J. Power Sources 196 (2011) 9270–9275.
[24] C. Jung, C.M. Sanchez-Sanchez, C.-L. Lin, J. Rodriguez-Lopez, A.J. Bard, Anal. Chem. 81 (2009) 7003–7008.
[25] M. Yin, Q. Li, J.O. Jensen, Y. Huang, L.N. Cleemann, N.J. Bjerrum, W. Xing, J. Power Sources 219 (2012) 106–111.
[26] W. Zhou, J.Y. Lee, J. Phys. Chem. C 112 (2008) 3789–3793.
[27] G. Hu, F. Nitze, H.R. Barzegar, T. Sharifi, A. Mikołajczuk, C.-W. Tai, A. Borodzinski, T. Wågberg, J. Power Sources 209 (2012) 236–242.
[28] X. Chen, G. Wu, J. Chen, X. Chen, Z. Xie, X. Wang, J. Am. Chem. Soc. 133 (2011) 3693–3695.
[29] H. Lu, Y. Fan, P. Huang, D. Xu, J. Power Sources 215 (2012) 48–52.
[30] R.M. Crooks, M. Zhao, L. Sun, V. Chechik, L.K. Yeung, Acc. Chem. Res. 34 (2001) 181–190.
[31] R.W. Scott, O.M. Wilson, R.M. Crooks, J. Phys. Chem. B 109 (2005) 692–704.
[32] B. Chandler, J. Gilbertson, in: L. Gade (Ed.), Dendrimer Catalysis, Springer, Berlin, Heidelberg, 2006, pp. 97–120.
[33] G.R. Newkome, C.D. Shreiner, Polymer 49 (2008) 1–173.
[34] C.N.R. Rao, A.K. Sood, K.S. Subrahmanyam, A. Govindaraj, Angew. Chem. Int. Ed. 48 (2009) 7752–7777.
[35] A.K. Geim, K.S. Novoselov, Nat. Mater. 6 (2007) 183–191.
[36] A.K. Geim, Science 324 (2009) 1530–1534.
[37] W.S. Hummers Jr., R.E. Offeman, J. Am. Chem. Soc. 80 (1958), 1339–1339.
[38] W.R. Collins, E. Schmois, T.M. Swager, Chem. Commun. 47 (2011) 8790–8792.
[39] E. Buhleier, W. Wehner, F. Vögtle, Synthesis 2 (1978) 155–158.
[40] R. Moors, F. Vögtle, Chem. Ber. 126 (1993) 2133–2135.
[41] M.P. Kapoor, Y. Kasama, T. Yokoyama, M. Yanagi, S. Inagaki, H. Nanbu, L.R. Juneja, J. Mater. Chem. 16 (2006) 4714–4722.
[42] A. Bosman, H. Janssen, E. Meijer, Chem. Rev. 99 (1999) 1665–1688.

[43] M.P. Seah, I.S. Gilmore, S.J. Spencer, J. Electron. Spectrosc. Relat. Phenom. 120 (2001) 93–111.
[44] L. Guczi, Z. Schay, G. Stefler, F. Mizukami, J. Mol. Catal. A Chem. 141 (1991) 177–185.
[45] D. Sun, V. Mazumder, Ö. Metin, S. Sun, ACS Nano 5 (2011) 6458–6464.
[46] T. Mallát, J. Petró, S. Szabó, L. Marczis, J. Electroanal. Chem. Interfaces 208 (1986) 169–173.
[47] R.W. Scott, O.M. Wilson, S.-K. Oh, E.A. Kenik, R.M. Crooks, J. Am. Chem. Soc. 126 (2004) 15583–15591.
[48] L. Zhang, Y. Tang, J. Bao, T. Lu, C. Li, J. Power Sources 162 (2006) 177–179.
[49] G. Chen, M. Liao, B. Yu, Y. Li, D. Wang, G. You, C.-J. Zhong, B.H. Chen, Int. J. Hydrogen Energy 37 (2012) 9959–9966.
[50] R.D. Morgan, A. Salehi-khojin, R.I. Masel, J. Phys. Chem. C 115 (2011) 19413–19418.
[51] L. Dai, S. Zou, J. Power Sources 196 (2011) 9369–9372.
[52] H. Lee, S.E. Habas, G.A. Somorjai, P. Yang, J. Am. Chem. Soc. 130 (2008) 5406–5407.
[53] H. Hosseini, H. Ahmar, A. Dehghani, A. Bagheri, A.R. Fakhari, M.M. Amini, Electrochim. Acta 88 (2013) 301–309.
[54] Y. Wang, B. Wu, Y. Gao, Y. Tang, T. Lu, W. Xing, C. Liu, J. Power Sources 192 (2009) 372–375.
[55] A.J. Bard, L.R. Faulkner, Electrochemical Methods: Fundamentals and Applications, Wiley, New York, 2001.
[56] K.V. Kordesch, G.R. Simader, Chem. Rev. 95 (1995) 191–207.
[57] Z.-L. Wang, J.-M. Yan, H.-L. Wang, Y. Ping, Q. Jiang, Sci. Rep. 2 (2012), 598–563.
[58] X. Zhou, Y. Huang, W. Xing, C. Liu, J. Liao, T. Lu, Chem. Commun. (2008) 3540–3542.